Electronic Supplementary Information

Highly Efficient Monolithic Perovskite Silicon Tandem Solar Cells: Analyzing the Influence of Current Mismatch on Device Performance

Eike Köhnen[a], Marko Jošt[a], Anna Belen Morales-Vilches[b], Philipp Tockhorn[a], Amran Al-Ashouri[a], Bart Macco[cd], Lukas Kegelmann[a], Lars Korte[d], Bernd Rech[d], Rutger Schlatmann[b], Bernd Stannowski[b] and Steve Albrecht[ae]

[a.] Helmholtz-Zentrum Berlin für Materialien und Energie GmbH, Young investigator group Perovskite Silicon Tandem Solar Cells, 12489 Berlin, Germany
[b.] Helmholtz-Zentrum Berlin für Materialien und Energie, PVcomB, 12489 Berlin, Germany
[c.] Department of Applied Physics, Eindhoven University of Technology, P.O. Box 513, 5600 MB Eindhoven, The Netherlands.
[d.] Helmholtz-Zentrum Berlin für Materialien und Energie GmbH, Institute for Silicon Photovoltaics, 12489 Berlin, Germany
[e.] Technical University Berlin, Faculty IV– Electrical Engineering and Computer Science, 10587 Berlin, Germany

# 1. Measured optical and electrical properties of IZO

Supplementary note 1

As a front contact, IZO was recently used in perovskite/silicon tandem solar cells.[1,2] In comparison to ITO, it already has superior optoelectrical properties when being deposited at room temperature and does not need to be annealed above 200 °C,[3,4] which would harm both the perovskite and SHJ solar cells. Besides the deposition temperature, IZO layer properties can be tuned by adding oxygen gas during the process. This leads to a reduction of oxygen vacancies, affecting conductivity and transparency as depicted in Figure S1. By adding oxygen, the vacancies, which contribute two electrons per defect,[5,6] are occupied. The lower carrier density leads to a reduction of the free carrier absorption especially in the NIR, but also to narrowing of the optical band gap due to the Burstein-Moss effect. Additionally, the mobility increases up to $46\,cm^2\,V^{-1}\,s^{-1}$, when adding up to $0.25\,\%_{vol}$ oxygen. As the resistivity, the inverse product of mobility and carrier density, is rather constant in this range, the optical properties are the decisive factor. The current density loss due to the absorption of IZO is calculated and displayed in the legend of Figure S1. As a minimum loss of $1.18\,mA\,cm^{-2}$ is achieved for $0.20\,\%_{abs}$ (grey line in Figure S1b) oxygen and 100 nm, we decided this to be an optimum for our design.

a)

b)
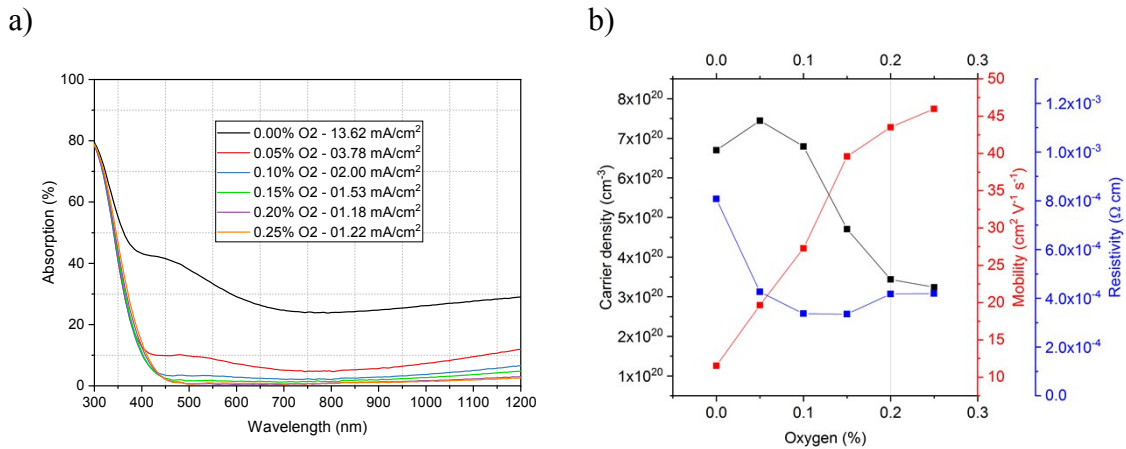

Figure S1: a) Absorption spectra of IZO films deposited on glass at room temperature with nominal thickness of 100 nm and different amounts of oxygen gas added into the sputter chamber. b) Carrier density, mobility and resistivity extracted from Hall-measurements for the IZO films shown in a). For the tandem solar cell, $0.2\,\%_{vol}$ oxygen (grey line) is added to the sputter chamber.

2. Schematic design of the tandem solar cell

Aperture mask

TCO / back contact / ARC

Contact patch

Metal frame
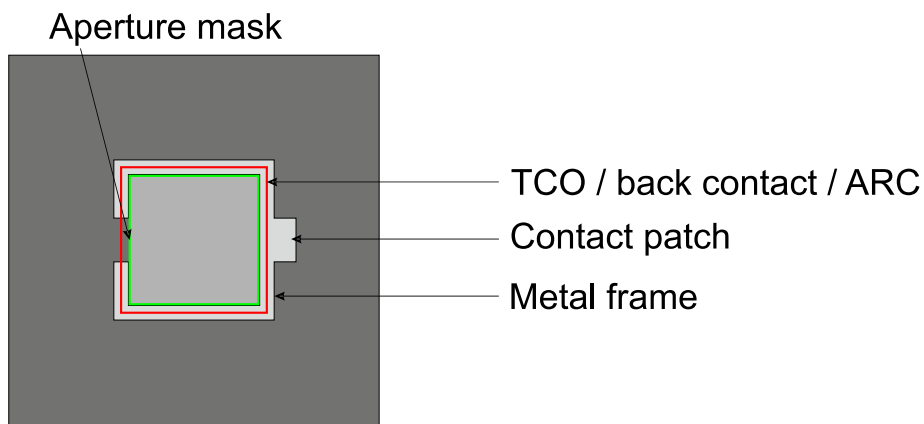
Figure S2: Schematic design of a tandem solar cell on a 25.0 x 25.0 cm^2 silicon substrate used in this study. The back contact, TCO between the sub-cells, front TCO and antireflective coating is deposited partially with an area of 1 x 1 cm^2 as indicated by the red square. To extract the carriers, the front metal frame needs to be in contact with the TCO and therefore it needs to be partially inside of the TCO-square. The inner square of the metal frame is 0.9 x 0.9 cm^2. The aperture mask (green square), used for measuring the JVs, reduced the size of illuminated area to 0.7709 cm^2

3. Further certification results including MPP track
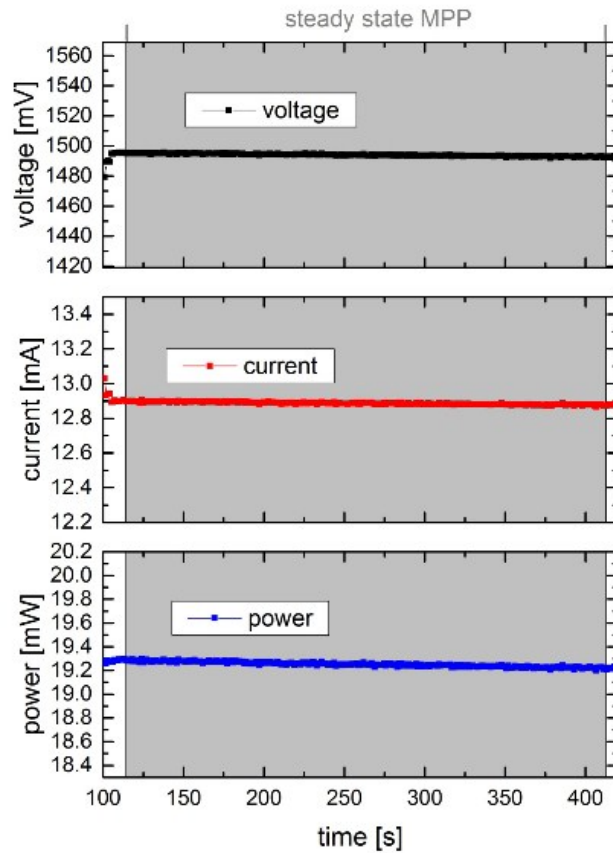
		Vorwärtsrichtung / forwards scan direction		Rückwärtsrichtung / reverse scan direction		MPP-Tracking / MPP-Tracking	
V_{oc}	=	(1780.8 ± 11.9) mV		(1777.9 ± 11.9) mV			
I_{SC} (Ed.2 - 2008)	=	(13.73 ± 0.26) mA		(13.73 ± 0.26) mA			
I_{MPP}	=	12.92	mA	12.91	mA	(12.89 ± 0.33) mA	
V_{MPP}	=	1488.2	mV	1481.9	mV	(1494.0 ± 25.2) mV	
P_{MPP}	=	19.24	mW	19.14	mW	(19.25 ± 0.51) mW	
FF	=	78.64	%	78.36	%		
η	=	24.95	%	24.82	%	(24.97 ± 0.73) %	

Figure S3 MPP track of a monolithic perovskite/silicon tandem solar cell, measured and certified by Fraunhofer ISE. With an area of $0.7709\,cm^2$, the stabilized efficiency is 24.97 % (average value of the last 300 s), as can be seen in the table below. Additionally it has to be highlighted that the forward and reverse scan direction show very similar performances indicating virtually hysteresis-free characteristics.

4. Optical simulation of the stack used for certified tandem cell
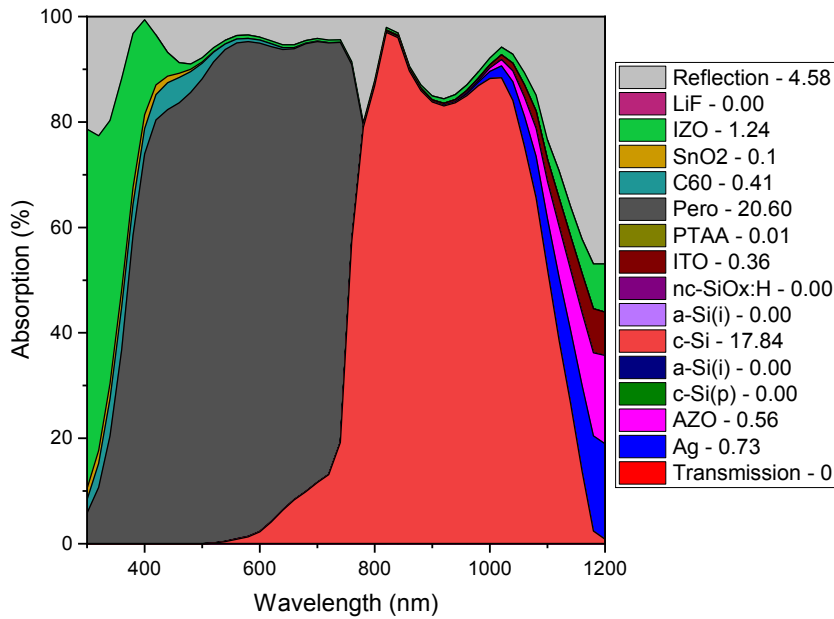
Figure S4: Simulated absorption and reflection spectra of the monolithic perovskite/silicon tandem solar cell from Figure 2 in the main text. The legend includes the current density (mA cm^{-2}), which is generated in the perovskite and silicon sub cell or lost due to reflection and parasitic absorption in each layer assuming AM1.5G incident illumination. The simulation is done with GenPro4[7] with n/k data sets as reported previously[8] and thicknesses determined via SEM, profilometry or spectroscopic ellipsometry.

5. Optical simulation for different ALD deposition temperatures of SnO$_2$

a)
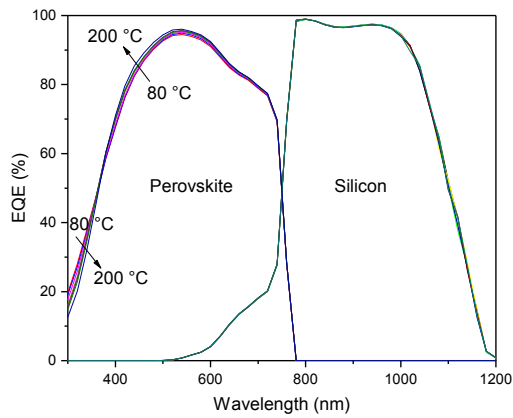
b)
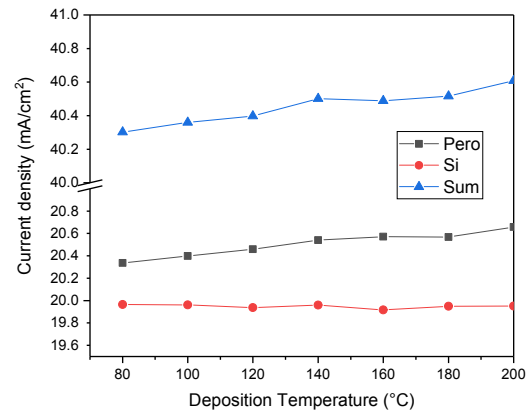
Figure S5: Simulation of a monolithic perovskite/silicon tandem solar cell with GenPro4.[7] The optical parameters of SnO$_2$, deposited at temperatures at 80 °C to 200 °C were changed, whereas all other optical parameters and thicknesses are constant. A lower deposition temperature leads to a higher EQE in the UV-range but simultaneously lowers the EQE above 370 nm (a). In the practical relevant range from 80 °C to 120 °C the sum increases just by 0.1 mA cm^{-2} (b). Sharing this to the sub-cells, this would lead to a current density increase of just 0.05 mA cm^{-2}.

6. Measured influence of the ALD temperature of SnO_2 for semitransparent perovskite top cells

a)

b)
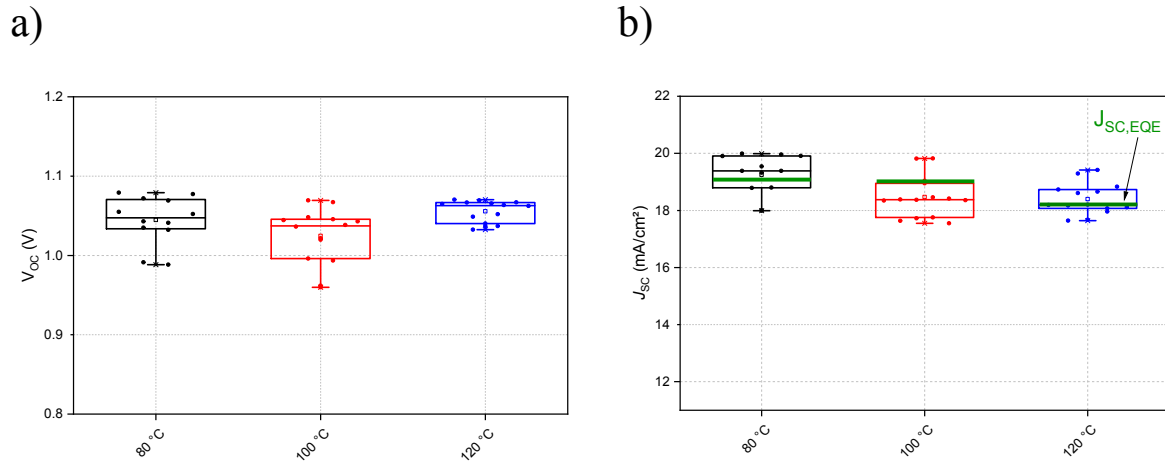
Figure S6: V_{OC} (a) and J_{SC} (b) of semitransparent p-i-n perovskite solar cells with SnO_2 deposited at temperatures ranging from $80\,°C$ to $120\,°C$. The cell architecture is equal to the top cell of a tandem cell without the anti-reflection coating. The cells are illuminated through the IZO layer. The green bars in b) indicate the J_{SC} calculated from the measured EQE for AM1.5G illumination.

7. Optical simulation for different front IZO thicknesses

a)
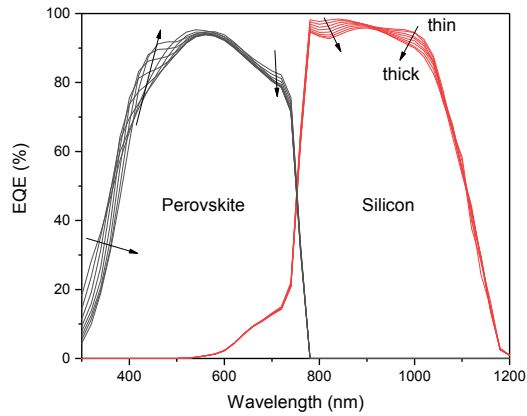
b)

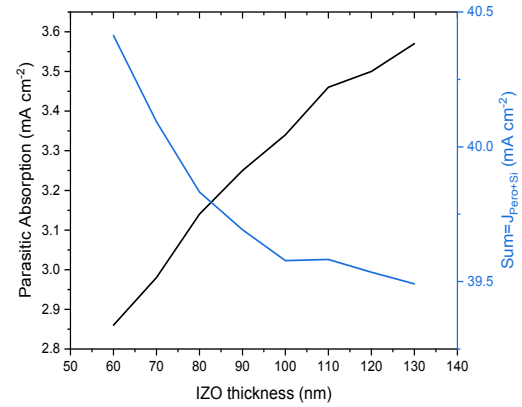**Figure S7**: Simulation of a perovskite/silicon tandem solar cell with varying thickness of the IZO layer. a) Simulated absorption of the light in the perovskite and the silicon sub cells varying the IZO thicknesses from 60 nm to 130 nm. The arrows show the trend from thin to thick IZO. b) Calculated parasitic absorption and cumulative currents $J_{Pero+Si}$ of the sub cells. Reducing the thickness leads to a reduced parasitic absorption and therefore a higher $J_{Pero+Si}$.

8. Optical simulation for different perovskite thicknesses

a)
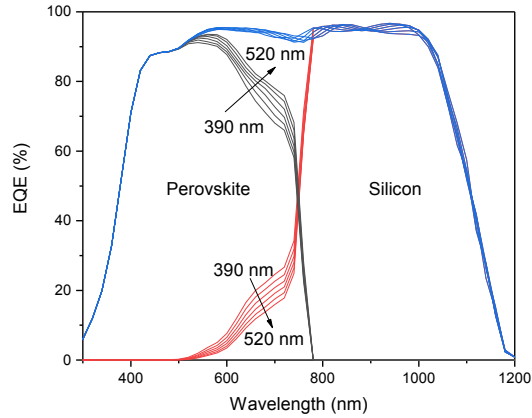
b)
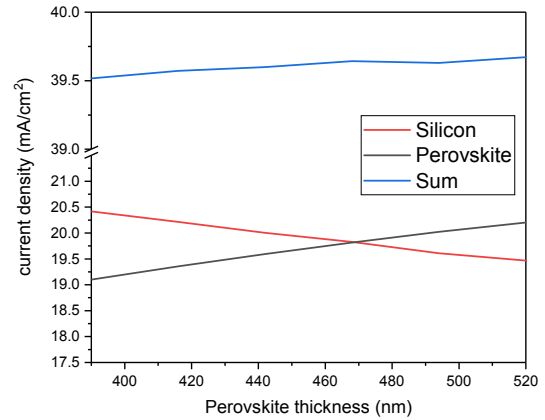
Figure S8: Simulation of a tandem solar cell with varying perovskite thickness. With changing the thickness (between 390 nm and 520 nm), the generated currents in the sub cells can be adjusted. a) Simulated absorption in the perovskite (black) and silicon (red) sub cells. Also the sum (blue) of the sub cells is shown, which hardly changes with the perovskite thickness. b) Calculated photogenerated current density in the sub-cells using the AM1.5G illumination. As the lowest current density approximately determines the J_{SC} in the total tandem cell, a maximum J_{SC} is expected for a perovskite thickness of around 470 nm.

9. EQE spectra of the individual single junction solar cells
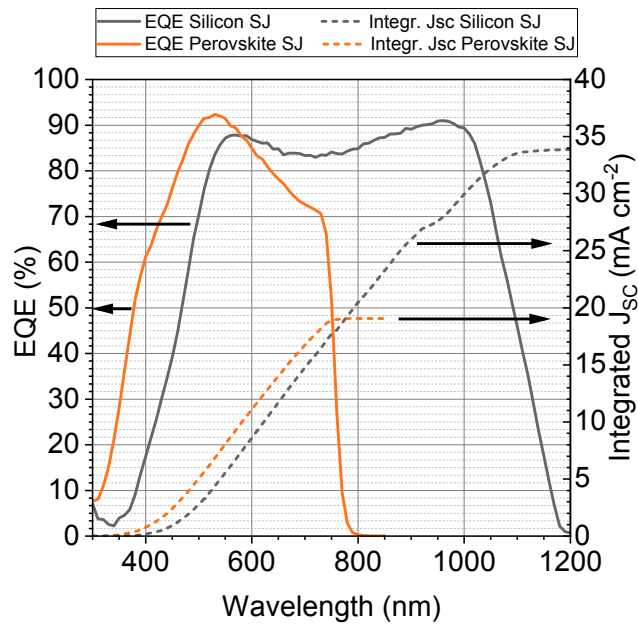
Figure 9: EQE spectra of single junction perovskite and silicon solar cells including integrated Jsc for AM1.5G illumination. The perovskite solar cell is a semitransparent cell with IZO as top layer, i.e. no antireflective coating is utilized. The EQE is measured through the IZO-side in substrate configuration as it is done in the tandem solar cell. A similar but opaque perovskite single junction solar cell is already published by Magomedov *et al.*[9]. The herein utilized silicon single junction solar cell is similar to the bottom cell used in our tandem stack. Only the nc-SiOx:H is 80 nm instead of 95 nm thick, which does not have a major impact on the overall performance. A similar silicon single junction solar cell was published by Mazzarella *et al.*[10]. Note, that for both, the perovskite and silicon cell, neither an antireflective coating is used nor the optical properties reflect that of the tandem integrated sub-cells as different absorption and interference features occur.

10.   Stability analysis of the tandem solar cell
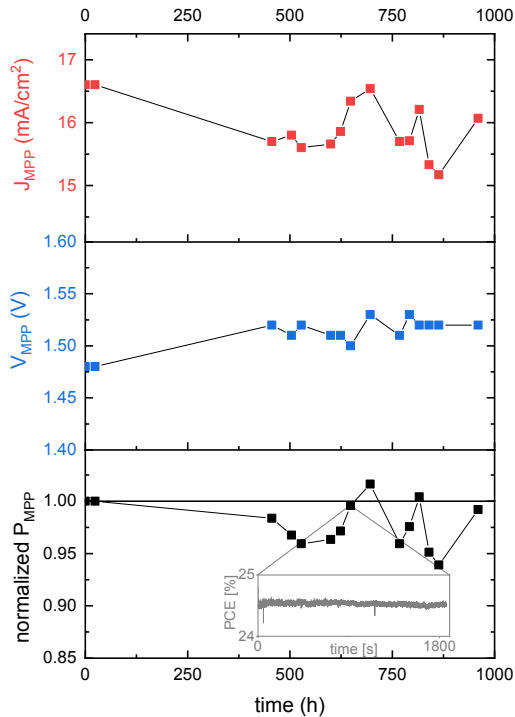
Figure S10: Stability study of an encapsulated monolithic tandem solar cell at 25 °C, ambient humidity and AM1.5G illumination. The initial values are $V_{MPP} = 1.48$ V, $J_{MPP} = 16.6$ mA cm^{-2}, PCE = 24.6 %. The PCE or power density follows the fluctuation of J_{MPP}, which is most likely a result of a fluctuating intensity. Nevertheless, the PCE did not drop below 93 % of its initial value after 1000 h. The inset shows the MPP tracking on day 27 after encapsulation. More details can be found below in Supplementary note 2.

Supplementary note 2

For stability measurements, we encapsulated a tandem solar cell, which was fabricated 23 days before and measured several times in ambient conditions. Before encapsulation, the stabilized efficiency was 26 % with $V_{MPP} = 1.45$ V and $J_{MPP} = 17.88$ mA cm^{-2}. It is encapsulated between two glasses and edge-sealed with an UV curable glue. Two copper stripes are used to connect the front and rear contact, respectively. Between the 30 minutes MPP tracks measured under standard test conditions, the sample was stored in ambient conditions. Summing up all measurements, the cell was measured for about 9.4 h. While the individual MPP tracks are stable (shown as an inset), the power has some variation unfortunately. This stems most likely from a fluctuating intensity of the sun simulator on different days (despite being calibrated) leading to fluctuating J_{MPP}. When taking the lowest measured value, the power density did not drop below 93 % after 1000 h. The last measured value is above 99 % of the initial performance.

11. Experimental tandem results for reduced front IZO thickness

a)

b)
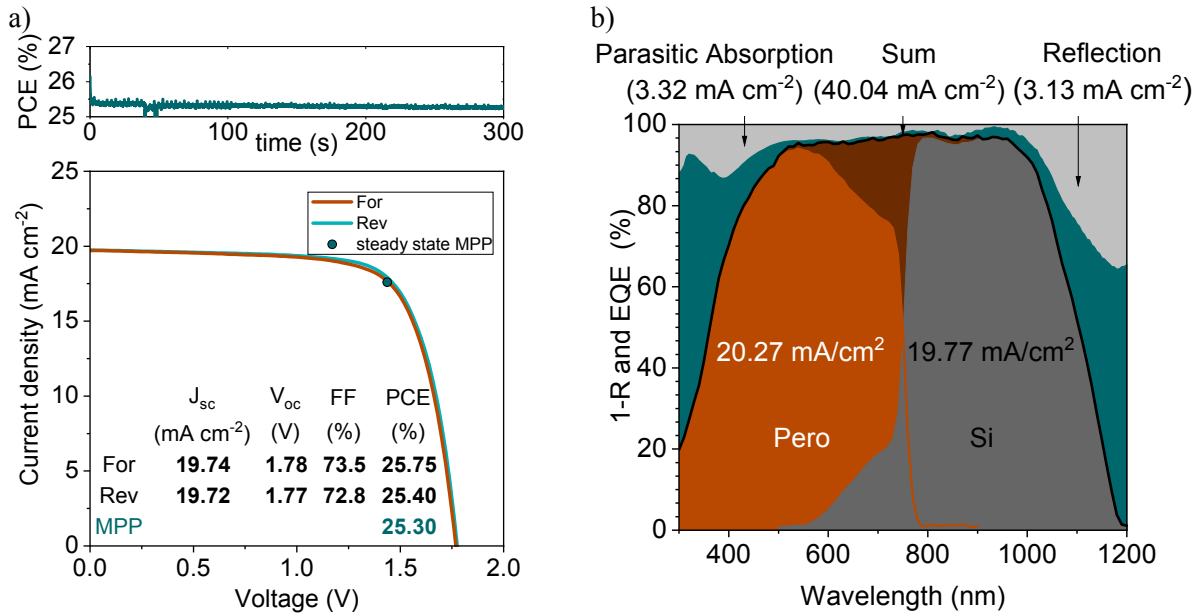
Figure S11: a) JV curve of an optimized monolithic perovskite/silicon tandem solar cell. This cell has the highest J_{SC}, measured within this work. b) EQE measurement of an optimized tandem solar cell gives a very high current density $J_{SC,EQE}$ of 19.77 mA cm^{-2}. This is comparable to the best tandem solar cell on textured silicon.[1] The sum already exceeds 40 mA cm^{-2}.

12. Measured tandem performance as function of current mismatch
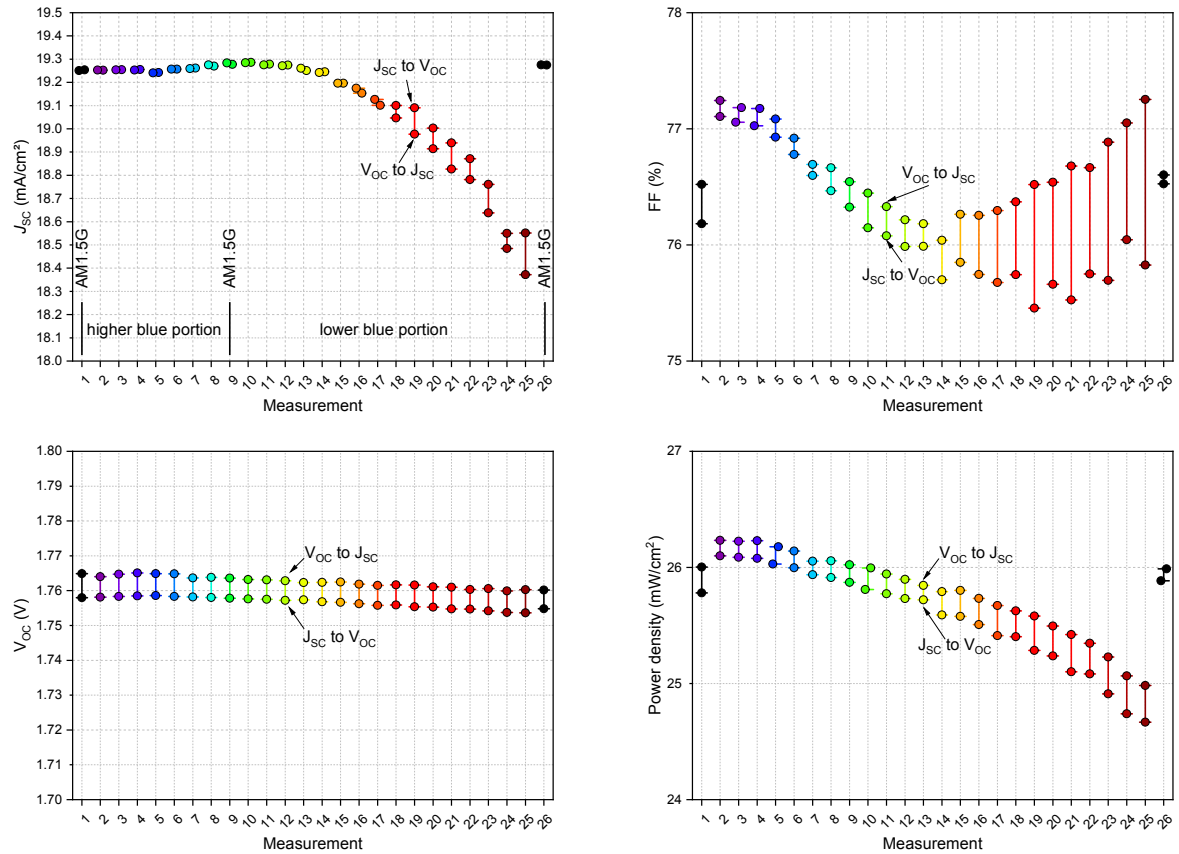
Figure S12: Parameters of a tandem solar cell illuminated with different spectra. By changing the intensity of two blue LEDs, we changed current generation in the perovskite sub cell. Starting from measurement no. 2 with the highest portion of blue light, the blue light is continuously decreased passing the AM1.5G at measurement no. 9 and decreased further until measurement no. 25. Before and after this series, a *J-V* was recorded under AM1.5G illumination to ensure that neither the cell degraded nor the spectrum shifted (measurement no. 1 and 26). In the main text in Figure 5 only the V_{OC} to J_{SC} (reverse scan) measurements are shown.

13.   Calculating the integrated intensity of the measured spectra

Supplementary note 3

As the utilized LED spectra are recorded just between 330 nm and 1087 nm, they need to be extended in order to calculate the integrated intensity (input power) and therefore the efficiency in Figure 5d in the main text. As measurement no. 1 in the series is measured close to AM1.5G conditions, the recorded spectrum no. 1 is used as a reference. Each other spectrum used, with more or less blue light, is then divided by spectrum no. 1 leading to a correction factor for each wavelength (factor function). Figure S13 shows the spectrum no. 1, spectrum no. 2 and the factor function for spectrum no. 2. Below 330 nm and above 1087 nm, the factor is set to 1. Each factor function is multiplied with the correct AM1.5G (ASTM G173-03) spectrum. The integrated intensity is then calculated by integrating the new spectrum and used as input power for the resulting efficiency.
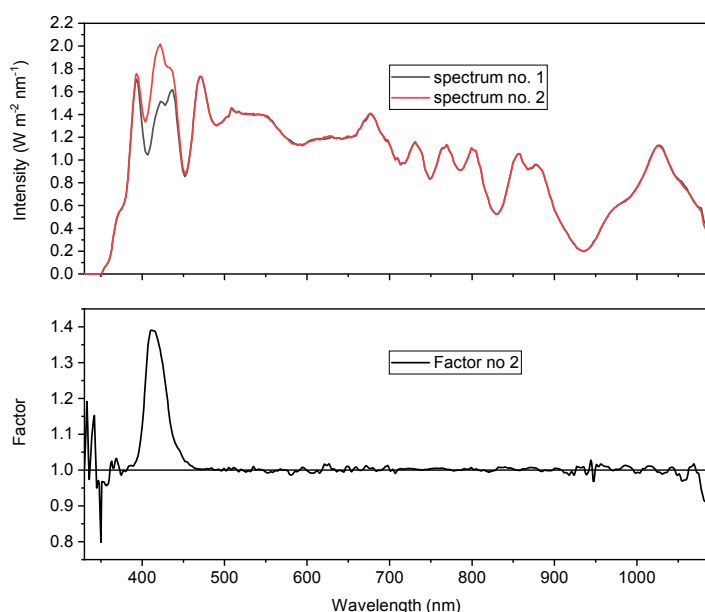
Figure S13: Spectrum recorded for measurement no. 1 and 2, respectively. The factor no. 2 is calculated by dividing spectrum no. 2 by spectrum no. 1.

14. Electrical simulations and comparison to experimental results

a)
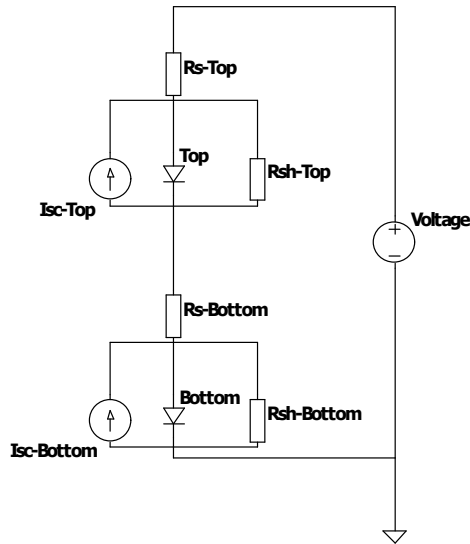
b)
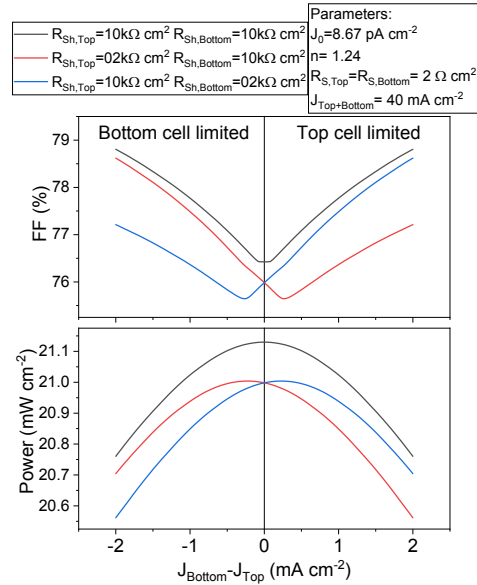
Figure S14: a) Equivalent circuit diagram utilized to describe a tandem solar cell using the simulation tool LTspice. The top and bottom cell, each consisting of a single diode model, are connected in series. b) Simulated FF and generated power as a function of the current density mismatch ($m = J_{Bottom} - J_{Top}$) for identical and asymmetric sub-cells. For the simulation of asymmetric sub-cells the shunt resistance R_{Sh} of the top and bottom cell is changed, as stated in the legend.

a)

b)

c)

d)

e)
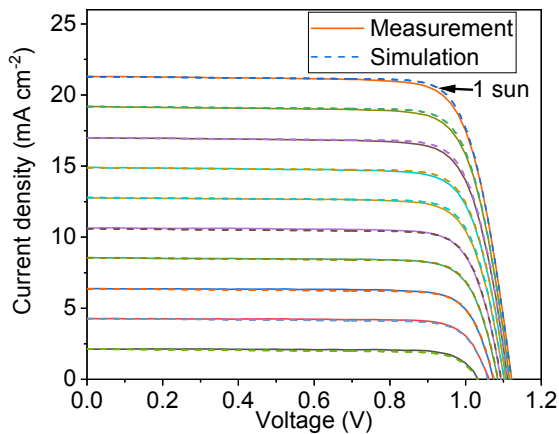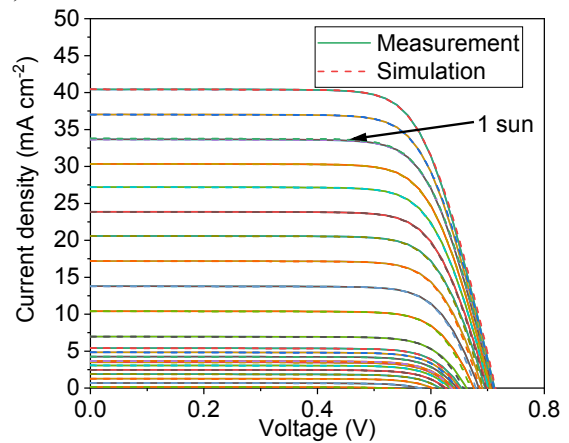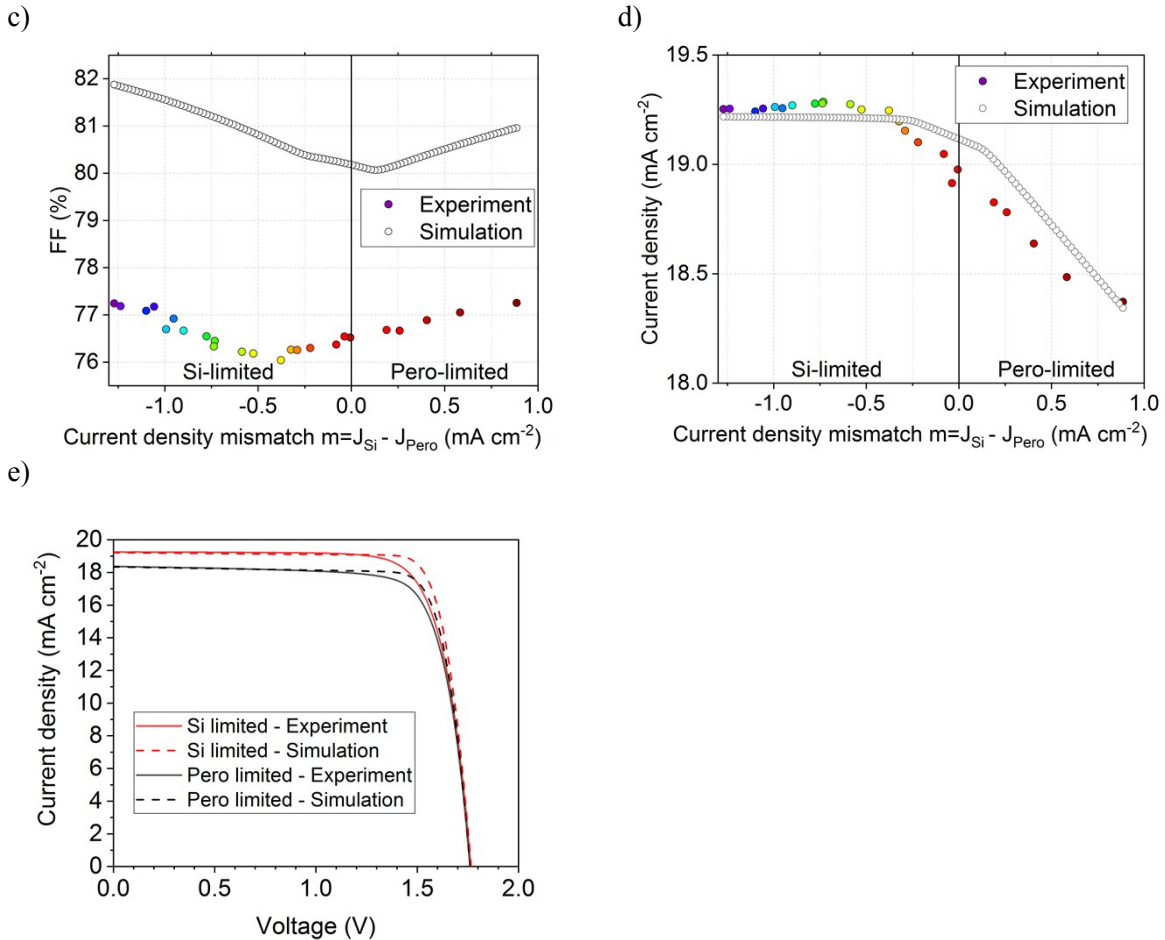
Figure S15: a) Opaque perovskite single junction solar cell measured at different intensities to extract electrical parameters for the single diode model. As this cell is opaque (i.e. a metal is used instead of a TCO), the series resistance due to the sheet resistance of the TCO is not included in this measurement and simulation. The corresponding fitting from electrical parametrization is also shown and the agreement is very good for the used range of intensities. b) Silicon single junction solar cell measured at different intensities to extract electrical parameters for the single diode equation. The corresponding fitting from electrical parametrization is also shown and is in very good agreement for the used range of intensities. c) FF as a function of the sub-cell current density mismatch from the experiment and simulation, respectively, using the electrical data from parametrized single junction solar cells as shown in Figure S15 a and b. Detailed information can be found in Supplementary note 4. d) Simulated and experimental short circuit current of the monolithic tandem solar cell as a function of current density mismatch. e) Simulated and experimental *J-V*s of the tandem solar cell measured at the most negative and most positive current mismatch *m* within this series.

Supplementary note 4

To simulate the FF dependency of a monolithic tandem solar cell in Figure S14b, two identical solar cells are connected in series with parameters displayed in the graphic. The shunt resistance is varied as stated in Figure S14b, while the top cell current is changed from $19 \, \text{mA cm}^{-2}$ to $21 \, \text{mA cm}^{-2}$ and the bottom cell current is adjusted in a way that the sum of the top and bottom cell is constantly at $40 \, \text{mA cm}^{-2}$.

For the electrical parametrization, single junction silicon and perovskite solar cells were fabricated with comparable contact design as used in the tandem stack; both cells are then measured at different intensities to extract the ideality factors. This is done by plotting V_{OC} against $\ln(J_{SC})$ and calculating the slope. This method results in ideality factors of $n_{Pero} = 1.46$ and $n_{Si} = 1.24$. The ideality factor agrees reasonably well for the perovskite[11] and is slightly higher as typically reported values for silicon[12] which we attribute to the contact design with a significant amount of electrically connected but not illuminated area. The saturation current J_0 is adjusted in a way that the experimental and simulated V_{oc} coincide: $J_{0,Silicon} = 8.6743$ pA cm^{-2}, $J_{0,Pero} = 26.78$ fA cm^{-2}. The series and shunt resistances R_S and R_{Sh} are adjusted in a way that the slope around V_{OC} and J_{SC} of the simulated J-Vs fit to the experimental results. This leads to the following values: $R_{S,Pero} = 2.976\ \Omega$ cm^2, $R_{Sh,Pero} = 4800\ \Omega$ cm^2, $R_{S,Si} = 2.08\ \Omega$ cm^2 and $R_{Sh,Si} = 9250\ \Omega$ cm^2. As no grid fingers are used, the high series resistances might be attributed to the sheet resistance of the front TCO. All values are additionally summarized in Table S1

To simulate the tandem J-V curves, both parameterized reference sub-cells are connected in series. As the V_{OC} of the monolithic tandem solar cell is slightly lower than the sum of the single junctions, which most likely stems from a lower V_{OC} of the perovskite sub-cell, the $J_{0,Pero}$ is changed to $J_{0,Pero} = 8.5$ fA cm^{-2}. Furthermore, the R_s is adjusted to the slope around V_{OC}, resulting in a sum of $R_{S,Si} + R_{S,Pero} = 3\ \Omega$ cm^2.

Table S1: Summarized parameters for the simulation with LTspice

	Perovskite as SJ (HZB)	Perovskite in Tandem (HZB)	Perovskite as SJ (PKU)[13]	Si as SJ and Tandem (HZB)	Si as SJ and Tandem (ISE)[14,15]
n	1.46	1.46	1.86	1.24	1.125
R_S	2.976 Ω cm^2	$R_{S,Si} + R_{S,Pero} = 3\ \Omega$ cm^2	3 Ω cm^2	2.08 Ω cm^2	0.001 Ω cm^2
R_{Sh}	4800 Ω cm^2	4800 Ω cm^2	20 kΩ cm^2	9250 Ω cm^2	9000 Ω cm^2
J_0	2.678 fA cm^{-2}	8.5 fA cm^{-2}	0.407 pA cm^{-2}	8.6743 pA cm^{-2}	0.665 pA cm^{-2}
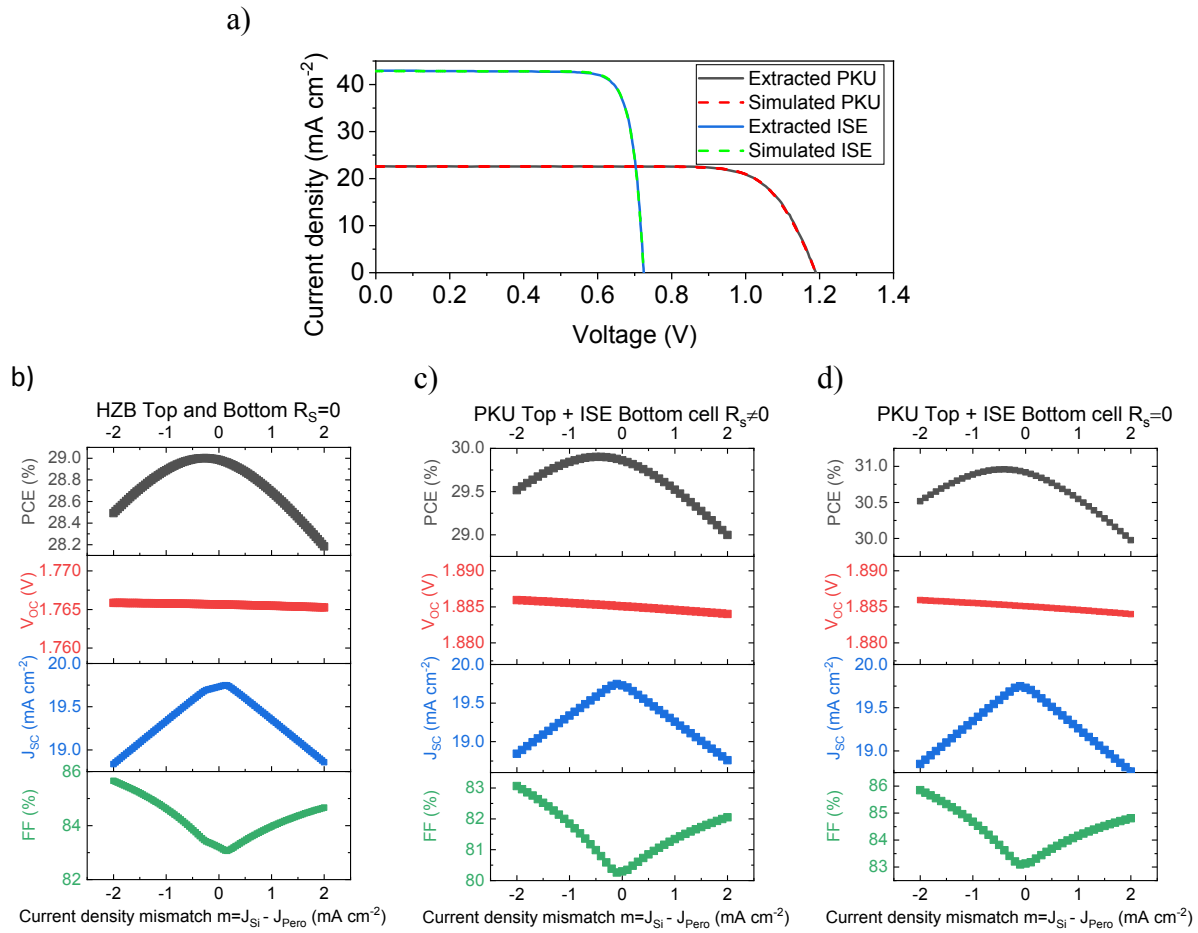
Figure S16: a) Extracted and simulated *J-V*s of a record p-i-n single junction perovskite[11] and both side contacted c-Si cell.[14,15] The parameters are displayed in Table S1. b) Simulation of the monolithic tandem solar cell shown in Figure S15 c-d with a series resistance of $R_s = 0 \, \Omega \, cm^2$ and a constant cumulative photogenerated current density $J_{Pero+Si}$ of 39.46 mA cm^{-2}. c) Simulation of a monolithic tandem solar cell using the parametrized record cell shown in a); The parameters used for the electrical simulation are shown in Table S1. A cumulative photogenerated current density of 39.46 mA cm^{-2} is assumed. d) Simulation of the same tandem solar cell as in c) but with a series resistance of $R_s = 0 \, \Omega \, cm^2$

Supporting Bibliography

1   F. Sahli, J. Werner, B. A. Kamino, M. Bräuninger, R. Monnard, B. Paviet-Salomon, L. Barraud, L. Ding, J. J. Diaz Leon, D. Sacchetto, G. Cattaneo, M. Despeisse, M. Boccard, S. Nicolay, Q. Jeangros, B. Niesen and C. Ballif, *Nat. Mater.*, 2018, **17**, 820–826.

2   J. Werner, F. Sahli, F. Fu, J. J. Diaz Leon, A. Walter, B. A. Kamino, B. Niesen, S. Nicolay, Q. Jeangros and C. Ballif, *ACS Energy Lett.*, 2018, **3**, 2052–2058.

3   H. Hosono and K. Ueda, *Springer Handbook of Electronic and Photonic Materials*, Springer US, Boston, MA, 2007.

4   M. Morales-Masis, S. De Wolf, R. Woods-Robinson, J. W. Ager and C. Ballif, *Adv. Electron. Mater.*, 2017, **3**, 1600529.

5   D. S. Ginley, *Handbook of Transparent Conductors*, Springer US, Boston, MA, 2011.

6   H. Kim, C. M. Gilmore, A. Piqué, J. S. Horwitz, H. Mattoussi, H. Murata, Z. H. Kafafi and D. B. Chrisey, *J. Appl. Phys.*, 1999, **86**, 6451–6461.

7   R. Santbergen, T. Meguro, T. Suezaki, G. Koizumi, K. Yamamoto and M. Zeman, *IEEE J. Photovoltaics*, 2017, **7**, 919–926.

8   M. Jošt, E. Köhnen, A. B. Morales-Vilches, B. Lipovšek, K. Jäger, B. Macco, A. Al-Ashouri, J. Krč, L. Korte, B. Rech, R. Schlatmann, M. Topič, B. Stannowski and S. Albrecht, *Energy Environ. Sci.*, 2018, **11**, 3511–3523.

9   A. Magomedov, A. Al-Ashouri, E. Kasparavičius, S. Strazdaite, G. Niaura, M. Jošt, T. Malinauskas, S. Albrecht and V. Getautis, *Adv. Energy Mater.*, 2018, **8**, 1801892.

10   L. Mazzarella, Y.-H. Lin, S. Kirner, A. B. Morales-Vilches, L. Korte, S. Albrecht, E. Crossland, B. Stannowski, C. Case, H. J. Snaith and R. Schlatmann, *Adv. Energy Mater.*, 2019, **1803241**, 1803241.

11   M. Stolterfoht, C. M. Wolff, Y. Amir, A. Paulke, L. Perdigón-Toro, P. Caprioglio and D. Neher, *Energy Environ. Sci.*, 2017, **10**, 1530–1539.

12   K. Yoshikawa, H. Kawasaki, W. Yoshida, T. Irie, K. Konishi, K. Nakano, T. Uto, D. Adachi, M. Kanematsu, H. Uzu and K. Yamamoto, *Nat. Energy*, 2017, **2**, 17032.

13   D. Luo, W. Yang, Z. Wang, A. Sadhanala, Q. Hu, R. Su, R. Shivanna, G. F. Trindade, J. F. Watts, Z. Xu, T. Liu, K. Chen, F. Ye, P. Wu, L. Zhao, J. Wu, Y. Tu, Y. Zhang, X. Yang, W. Zhang, R. H. Friend, Q. Gong, H. J. Snaith and R. Zhu, *Science (80-.).*, 2018, **360**, 1442–1446.

14   M. A. Green, Y. Hishikawa, E. D. Dunlop, D. H. Levi, J. Hohl-Ebinger and A. W. Y. Ho-Baillie, *Prog. Photovoltaics Res. Appl.*, 2018, **26**, 3–12.

15   A. Richter, J. Benick, F. Feldmann, A. Fell, M. Hermle and S. W. Glunz, *Sol. Energy Mater. Sol. Cells*, 2017, **173**, 96–105.